Experimental Study on Long-Span Composite Floor Beams Subject to Fire: Baseline Data at Ambient Temperature

Lisa Choe[1], Selvarajah Ramesh[1], Matthew Hoehler[1], John Gross[1]

[1]National Institute of Standards and Technology, 100 Bureau Drive, Gaithersburg, MD 20899; email: lisa.choe@nist.gov; selvarajah.ramesh@nist.gov; matthew.hoehler@nist.gov; john.gross@nist.gov

ABSTRACT

The National Institute of Standards and Technology recently expanded its large-scale structural-fire testing capabilities in the National Fire Research Laboratory. A landmark test series is being conducted on long-span steel-concrete composite floor beams designed and constructed following U.S. building codes and standards. The test program consists of five 13 m span composite beams with one of two types of shear connections: bolted/welded double-angle connections or single plate shear connections. Two of the five specimens have slab continuity at the beam ends. This paper presents the results from a recent test on the composite beam conducted at ambient temperature. The experimentally measured behavior and flexural moment capacity will be used as a baseline to compare with the composite beams still to be tested under combined mechanical and fire load. The datasets produced are providing technical information necessary to advance performance-based design of composite floor systems in steel-framed buildings subject to fire.

INTRODUCTION

The National Institute of Standards and Technology (NIST) recently commissioned the newly expanded National Fire Research Laboratory (NFRL) to enable large-scale structural-fire experiments under controlled laboratory conditions (Bundy et al., 2015). As for its first structural-fire test program, the performance of mechanically loaded composite floor beam assemblies exposed to a structurally significant fire has been studied. The resulting datasets will serve as a technical information to improve the current practice of structural fire engineering and design of steel-framed buildings.

Composite floor systems were selected for this study because of their widespread use in construction. The WTC 7 investigation report (NIST, 2008) and a recent study by Flint et al. (2013) identified potential vulnerabilities of composite floor systems in uncontrolled fires that were related to structural layout, sources of thermal restraint, and connections. However, modeling long-span composite beams exposed to a fire is challenging, especially, when they were restrained by structural steel connections and surrounding framing. The system-level fire performance is attributed to not only the high-temperature behavior of individual elements such as a steel beam, a concrete slab, shear studs, and shear connections at the beam ends, but also the combined structural-fire interactions among them.

Although there have been some experimental studies on composite beams with fire load, most of the specimens tested in U.S. [e.g., Wellman et al. (2011); Selden et al. (2015); Alfawakhri

(2016)] were short span beams in the range of 4 m to 6 m. A series of stakeholder meetings led by NIST with researchers and industry experts identified that there is a significant need for data on composite floors beams with the beam length suitable for a modern office building, i.e., 10 m or longer. Hence, the focus of this test program is to study the fire performance of nominally 13 m long composite beams, which are restrained by shear connections and surrounding gravity frames, under real fire conditions.

A total of five composite test beams were designed and constructed in accordance with U.S. building codes and standards. Two different types of connections are used: (i) welded/bolted double angles and (ii) single plate connection (shear tab). Two of the five specimens have a slab continuity at the primary girders provided by rotationally restraining steel reinforcement in concrete slab extended beyond the support columns. Figure 1 shows a rendering of the test setup. For the specimens tested with fire, a compartment wall will be constructed around the specimens to confine the fire from the burners below the specimen. For the fire tests, three 1 m × 1.5 m natural gas burners will be used to generate a fire with a total heat release rate of 4 MW. Details about specimens and test setup are presented in the companion paper titled "Design and Construction of Long-Span Composite Beam Specimens for Large Structural-Fire Tests" included in this conference proceeding.

This paper presents the results from the composite beam test at ambient temperature. The measured behavior, failure mode, and flexural moment capacity will serve as a baseline to compare with the results from subsequent fire tests on the composite beams. The datasets produced by this research is providing technical information to better understand the fire performance of long-span composite floor beams and to advance performance-based design of composite floor systems in steel framed buildings subject to structurally-significant fire.

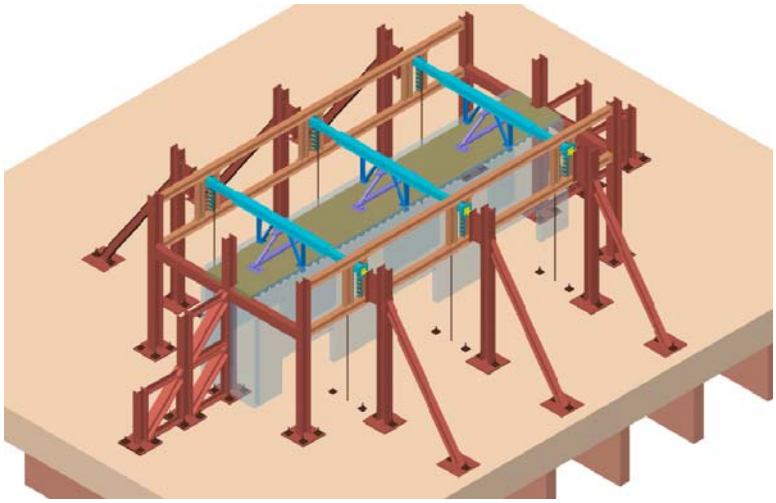

Figure 1 Rendering of the test setup.

TEST SETUP

Composite Beam and Shear connection

Design parameters of the composite beam specimen (e.g., design loads, beam spacing, concrete slab, reinforcement, and metal decking) were determined through surveys of U.S. structural engineering practitioners. Using values from the survey, the test beam was designed to represent a typical filler beam used in composite floor systems, in accordance with the current American National Standards Institute (ANSI) and American Institute of Steel Construction (AISC) ANSI/AISC 360 specification. The appropriate shear connection for gravity frames was selected using the AISC design tables. The complete design calculations were independently checked by AISC engineers to ensure the test beam was designed according to common U.S. practice. It should be noted that numerical values reported in this manuscript have two significant figures.

Figure 2a shows the cross-section of the composite beam specimen. A lightweight aggregate concrete with polypropylene fibers (PP) was cast over 7.6 cm deep fluted galvanized steel decking. The minimum specified compressive strength of the concrete was 28 MPa. The topping concrete measured 13 m by 1.8 m in plan. The steel deck units were installed with the flutes running perpendicular to the W18×35 beam made of American Society for Testing and Materials (ASTM) grade A992 steel. The thickness of concrete topping was 8.3 cm. For composite action, 19 mm diameter steel headed studs were welded at every flute spaced at 31 cm. The resultant percentage of composite action between the concrete slab and the steel beam, i.e., the total shear connection strength divided by the yield strength of the steel cross section, was 82 % with strong shear stud position. The slab was reinforced with a 6×6 W1.4×W1.4 welded wire fabric (9 mm^2 steel wires spaced at 15 cm in both the longitudinal and transverse directions), which was located at the mid-depth of a topping slab.

The test beam was supported by W12×106 columns via two L5×3×3/8 angles made of ASTM A36 steel (Figure 2b). Each angle was cut to the length of 23 cm. The angle legs on the face of support columns were shop-welded to a 1.9 cm thick sacrificial connection plate; the other legs were bolted to the web of the W18x35 beam using three ASTM A325 bolts with the diameter of 1.9 cm. The spacing of bolt holes was 7.6 cm. The gap between the sacrificial plate and the end of the steel beam was 1.3 cm.

Table 1 summarizes the mechanical properties of the steel used in the construction of the beam. Strength of all steel components were measured by ASTM E8 standard (2016). The concrete for this specimen came from two batches. The mean concrete compressive strengths – determined according to ASTM C39 (2017) – were 50 ± 1.8 MPa (west half of beam) and 54 ± 3.3 MPa (east half of beam) at the time of the ambient beam tests (290 days after casting). It is noted that standard uncertainties are reported throughout this paper (cover factor = 1).

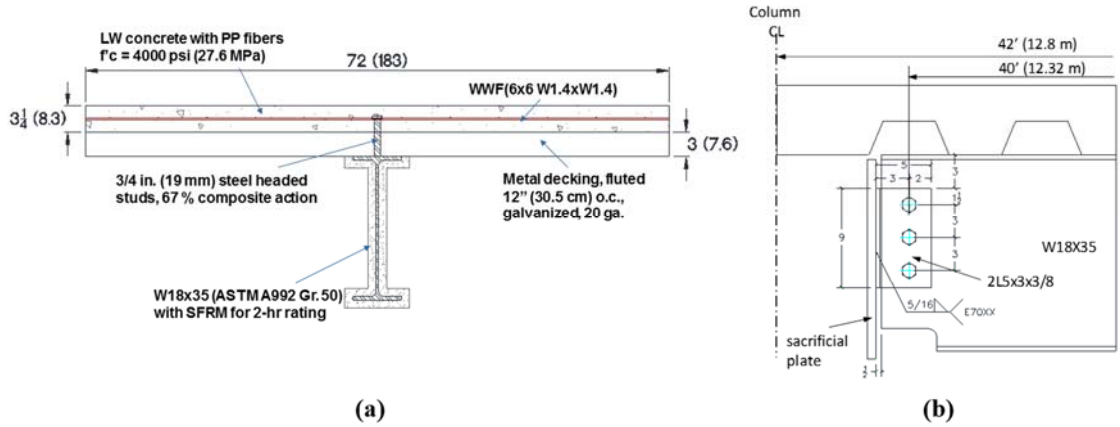

Figure 2 (a) Cross-section of the composite beam and (b) angle connection (connection dimensions in inches; 1 in. = 2.54 cm).

Table 1 Mechanical properties of steel components.

Material	ASTM Steel Designation	E (GPa)	F_y (MPa)	F_u (MPa)	e_u (%)
W18x35-Web	A992	200	370	470	19
W18x35-Flange	A992	210	350	470	19
Steel Angle	A36	200	380	510	17
Structural Bolt	A325	210	900	960	6
Shear Stud	A108	210	410	500	5
Wire Mesh	A1064	200	730	760	1

Note: E = Elastic modulus, F_y = Yield strength, F_u = Ultimate strength, e_u = Percent elongation at ultimate strength

Mechanical Loading System and Load Protocol

The test beam was subjected to a uniform floor load simulated by applying six equally-spaced point loads along the centerline of the beam (Figure 3a). The loading system consisted of three loading beams with rectangular tube section (9×7) which were hydraulically loaded at their ends using six actuators mounted below the strong floor of the test lab. The loading beams were guided such that they could only move vertically as the specimen deforms. Each loading beam was connected to the loading truss via clevis-pin assemblies. As the loading beam was loaded, each support of loading trusses transferred concentrated loads on the beam specimen. To prevent twisting of the test beam when loaded, the edges of the floor slab were laterally braced at the location of loading beams (Figure 3b). The 5×5 steel tubes were also used to provide vertical support at the east and west ends of slabs.

Figure 3c shows the applied load versus time relationship. All six actuators connected at the ends of three loading beams were programed such that they increased loads at a rate of 1.1 ± 0.053 kN/min. A total of three cycles of loading were applied to capture the full sequence of failure when the composite test beam was subjected to monotonically increasing flexural loads. The

plateaus at 11 kN, 22, kN and 44 kN during Cycle 1 were pauses to make strain measurements using fiber optics. Two actuators each connected to the same loading beam were also programmed to increase the actuator stroke (displacement) at the same rate as the test beam deformed, and therefore the loading beam was horizontally leveled throughout the test duration.

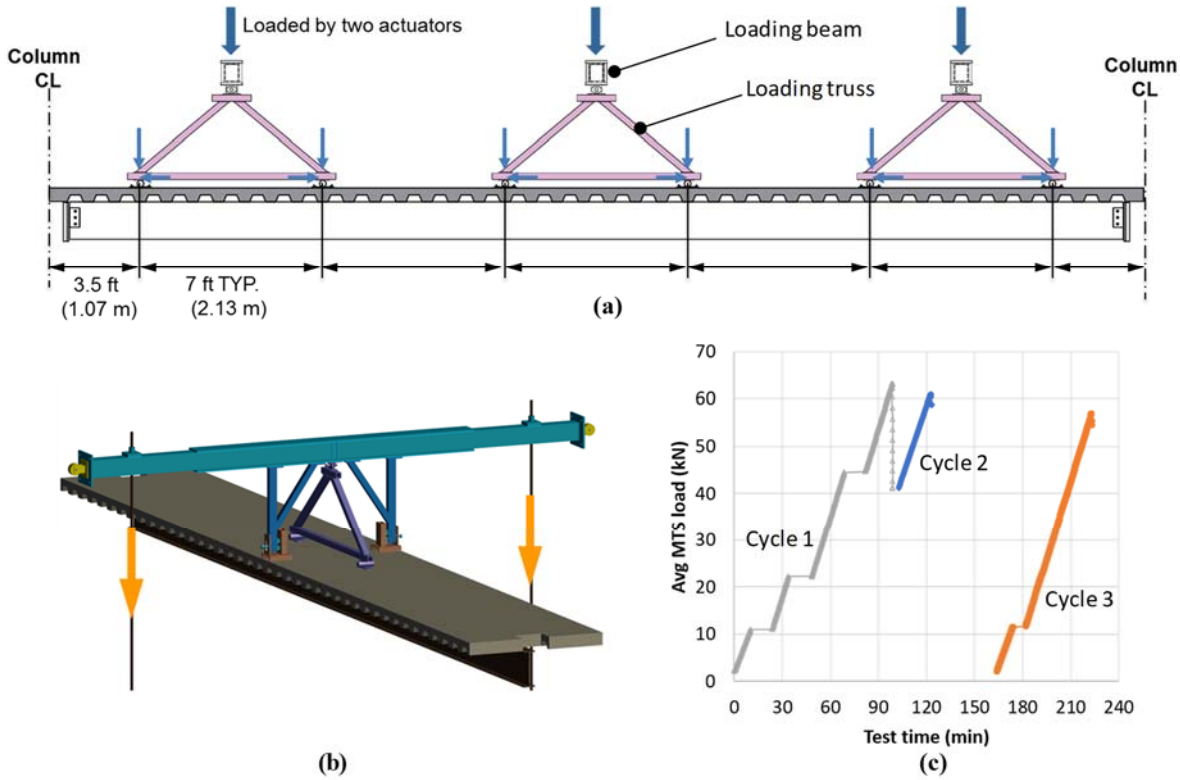

Figure 3 (a) Loading system (b) lateral brace, and (c) applied load time history.

Instrumentation and Measurement Uncertainty

Figure 4 shows the instrumentation layout to measure global and local behavior of the test beam at various locations. Linear strain gages were used to measure the section behavior of the test beam and angle connections. Linear displacement transducers were employed to measure the displacement of the concrete slab at the locations of point loads, the displacement of the bottom flange of the W18×35 steel beam at midspan, the slip of the concrete slab relative to the end of the steel beam, and the gap closure at the bottom coped web. Rotation transducers were installed to measure the end rotation of the test beam. Table 2 shows the estimated total expanded uncertainty in measurements with a coverage factor of 2 as defined in Taylor and Kuyatt (1994). Further details of individual sensors are presented in Choe et al. (2017).

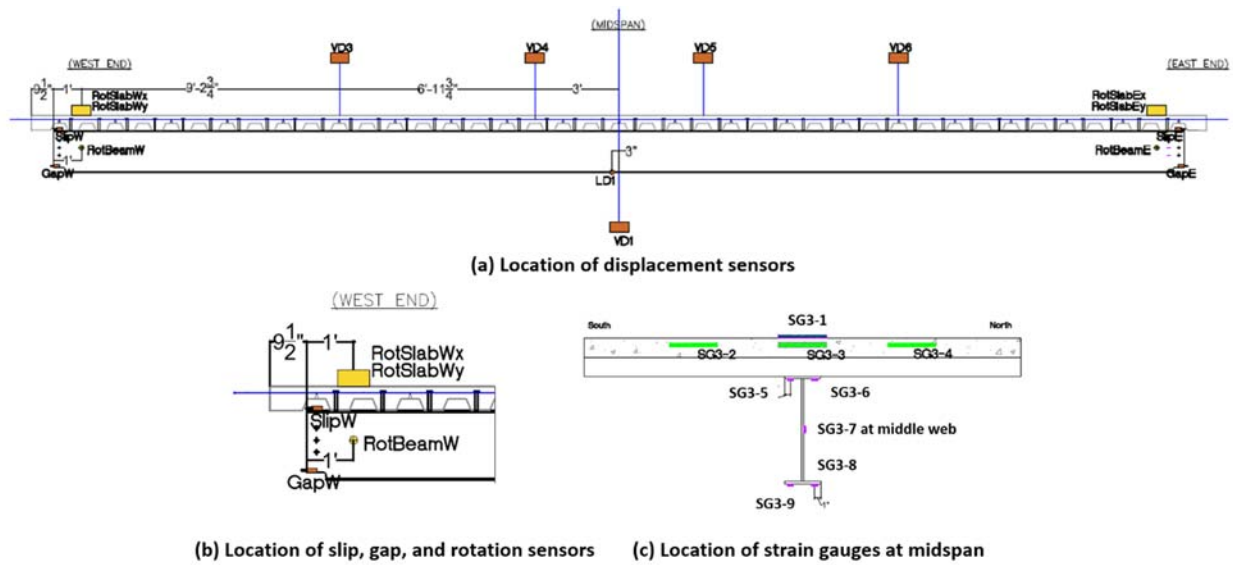

Figure 4 Location of sensors (a) displacement sensors (b) slip, gap, and rotation sensors, and (c) strain gages at midspan.

Table 2 Measurement uncertainty of sensors

Sensor description	Range (max)	Total Expanded Uncertainty[1]
Actuator Load cell	365 kN	±10 %
String potentiometer	760 mm	±15 %
Linear position sensor	38 mm	±2.0 %
Inclinometer	60°	±8 %
Strain gauge	50,000 με	±5 %

TEST RESULTS

Global Behavior

Figure 5a shows a photograph of the beam after the test. Figure 5b shows the average point load versus the displacement relation measured at the bottom flange of the steel beam at midspan. Figure 5c shows the change in the vertical displacement profile of the concrete slab during the first cycle of loading, and Figure 5d shows the maximum vertical displacement measured at the peak load of each cycle. It should be noted that the displacements in Figures 5c and 5d were measured from the top of the concrete slab.

[1] The uncertainty components included calibration, installation, random, and repeatability. The combined standard uncertainty was estimated by combining the individual uncertainties using root-sum-of-squares. The expended uncertainty was then computed by multiplying the combined uncertainty by a coverage factor of 2 corresponding to an approximately 95 % confidence interval.

As shown in Figure 5b, the flexural capacity of the test beam decreased with increasing number of loading cycles. During the first cycle, the vertical displacement of the beam was initially symmetric with respect to the midspan until the horizontal shear bond failure provided by headed studs was initiated at the west end (Figure 5c). After the first peak load of 63 ± 6.1 kN was achieved, the loads were manually relaxed to 40 kN, approximately. The second cycle was proceeded with the same load rate, and the specimen reached its second peak load of 61 ± 5.9 kN at which almost the west half of the beam lost the composite action. The third load cycle was resumed with the same load rate until the specimen collapsed following the complete weld fracture failure at the west angle connection. The third peak load was measured at 57 ± 4.1 kN, and the corresponding displacement at midspan was 360 mm, approximately $L/35$ where L is the beam span of 13 m. The values after ± symbol indicate the standard deviation of six point loads.

The horizontal shear failure (fracture of a shear stud) initiated at the west end also resulted the asymmetrical vertical displacement about the centerline of the test beam. At the end of the third cycle of loading, as shown in Figure 5d, a plastic hinging was formed at the section where the west support of the middle load truss was located (i.e., approximately 1 m from the beam centerline). The maximum vertical displacement of concrete slab at this location was 360 mm. With the lateral braces provided on the concrete slab at the location of three loading beams and the vertical supports at the east and west slab ends, the maximum lateral displacement of the beam specimen was 2.5 mm approximately.

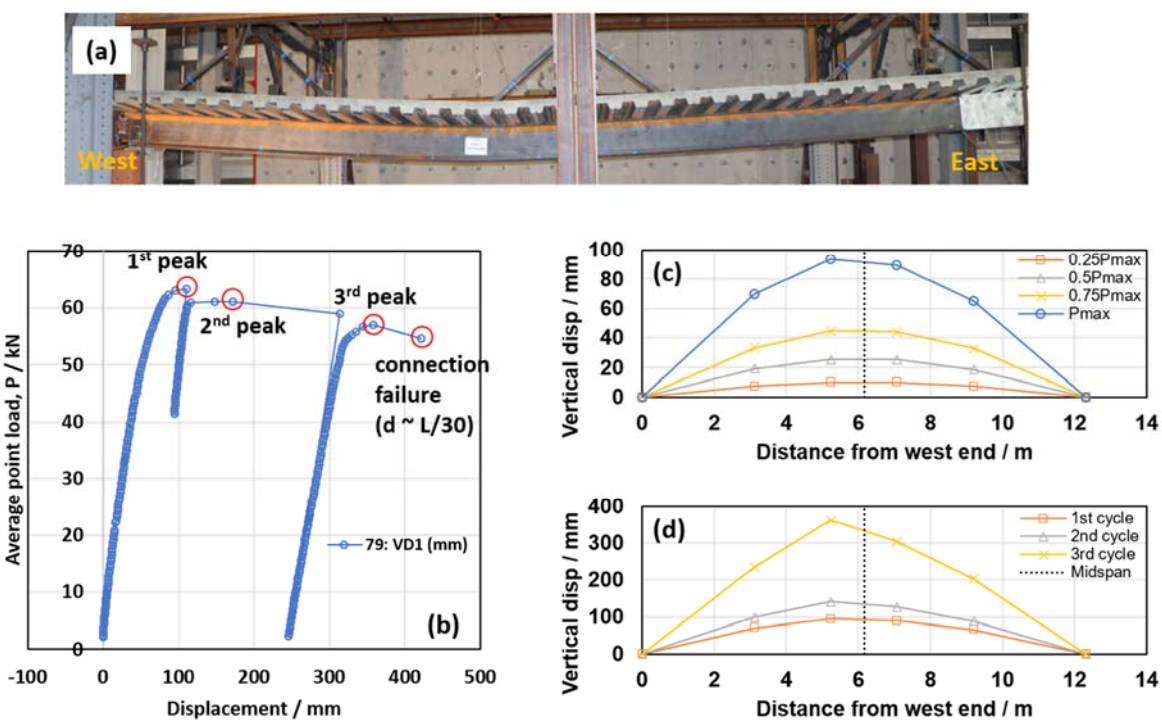

Figure 5 (a) Photograph of the beam after test, (b) total load versus displacement at midspan, (c) vertical displacement profile of the concrete slab, and (d) the maximum vertical displacement measured at the peak load of each cycle.

End Slip and Gap Closure

Figure 6 shows (a) the slip of the concrete slab relative to the end of the steel beam and (b) the change in gap distance between the column sacrificial plate and the bottom coped web as the test beam underwent multiple cycles of flexural loading. Those relative displacements (between two planes) were measured using spring-loaded displacement sensors at the locations shown in Figure 4b. At the west end, the end slip significantly increased (to nearly 30 mm) at the peak load of the second cycle (Figure 6a), which indicated the horizontal interaction failure between the concrete slab and the steel beam. However, the end slip at the east end remained below 0.85 mm until the test beam failed.

The initial gap distance from the bottom coped web to the face of the column sacrificial plate was designed to be about 13 mm in accordance with U.S. practice (Figure 2b). As shown in Figure 6b, the gap distance varied as the test beam was subjected to increasing point loads in each cycle of loading. The gap closure at the west end was significantly greater than the east end. When the west half of the beam lost the composite action, the non-composite steel beam section was subjected to large bending. Yet, the gap distance at both ends never decreased to zero (i.e., there was no bearing of the bottom copped web on the support column).

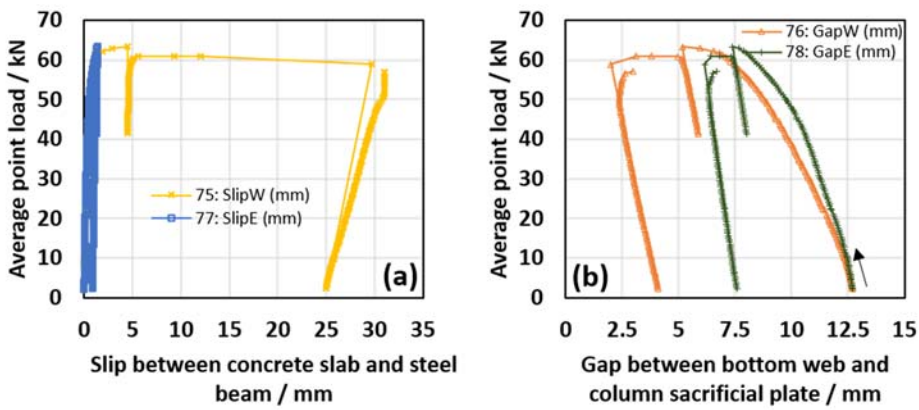

Figure 6 (a) Slip between concrete slab and steel beam and (b) gap distance between sacrificial plate and beam web.

Section Behavior

The section behavior induced by flexural loading was measured using strain gauges installed at various cross-sections along the beam span. This paper only focuses on the strain responses in the expected plastic hinge region subjected to maximum bending moments (i.e. between two point loads around the midspan). Figures 7a and 7b show the strain in the mid-section measured at various load levels during the first cycle and the close view of strains in compression zone (the top flange of the steel beam and concrete slab), respectively. The y-axis of each plot indicates the section depth measured from the bottom flange of the W18×35 steel beam. As shown, the steel beam was in tension and the concrete slab was in compression during the first cycle, as indicating that the neutral axis was located within the top flange. The maximum compressive strain

in concrete and the maximum tensile strain was 0.07 % and 0.2 % at the peak load of the first cycle.

Figures 7c and 7d show the strain distribution in the mid-section at each peak load of loading cycles and strains in the upper portion of the cross section, respectively. The neutral axis shifted downward to the steel beam section as the horizontal shear failure propagated into the midspan. At the end of the third cycle of loading, the specimen lost the horizontal shear interaction (between the concrete slab and the steel beam) which can be indicated by the presence of two neutral axes. The tensile strain was developed in the concrete slab. The top flange of the steel beam exhibited strain of 0.2 %, and the bottom flange failed by yielding with the maximum strain of 0.5 %.

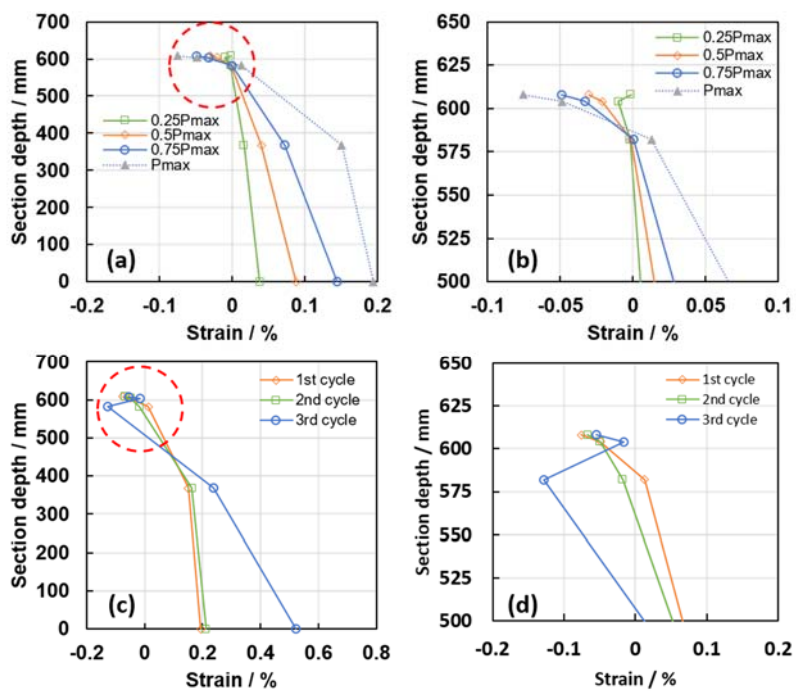

Figures 7 (a) Strain at midspan during first cycle, (b) strains in compression zone during first cycle, (c) strain distribution in the mid-section at each peak load of loading cycles and, (d) strains in in compression zone during different load cycles.

Connection Behavior

The performance of the steel angle connections was measured using strain gauges as shown in Figures 8a and 8b. Due to the page limit, this paper only presents the strains in the critical locations such as the top of the angle legs welded to the sacrificial plate on support columns (Figure 8c) and the top of the other legs of the same angle that was bolted to the beam web (Figure 8d). Since the connection behavior was complex, the load cycle number is shown in the graphs. As shown, the top of the angle leg on the column side exhibited compressive strains during the first two cycles of loading as indicating prying of the attached angles. The strain reversal occurred when fracture at the weld return was initiated at about 45 kN during the third cycle. The angles at the

east end developed more ductile behavior than the west end where the shear stud failure occurred. The maximum compressive strain was 0.83 % prior to strain reversal. On the other hand, the top of the angles bolted to the beam web at both east and west ends exhibited similar behavior. There was no significant increase in strains (less than 0.05 %) during the first cycle, and then tensile stresses, indicated by a positive slope in strain data, were developed during the last two cycles until weld fracture occurred.

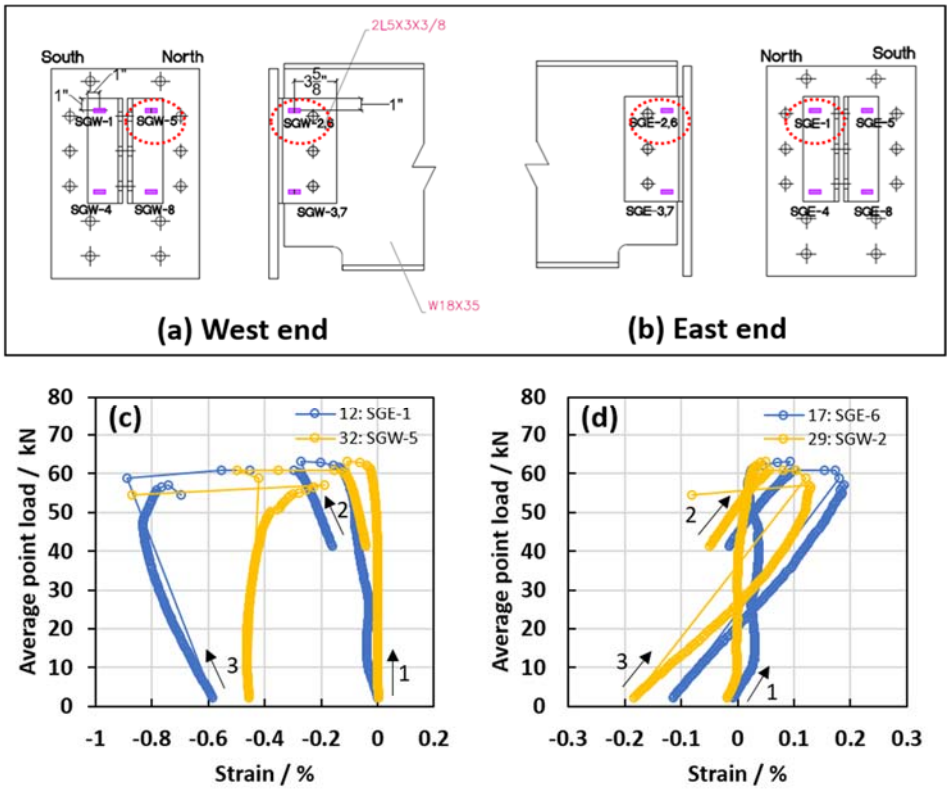

Figure 8 (a) Strain gage layout in the west connection, (b) strain gage layout in the east connection, (c) strains in the top the angle legs welded to the sacrificial plate, and (d) strains in the top of the angle legs bolted to the beam web.

Failure Mode

The sequence of failure in the test beam was identified through a series of load cycles in which the applied point loads were increased at a rate of 1.1 kN/min. The test specimen exhibited failure at the interface between the shear studs and the concrete when subjected to a monotonically increasing bending moment about its strong axis. This failure was initiated at the west end and then propagated toward the midspan (Figure 9a), presumably due to the slightly lower concrete strength at the west end of the specimen. As shown in Figure 9b, shear studs in this region deformed in the same direction of compressive forces by concrete slab subjected to flexural loading, and the last shear stud at the west end failed by steel rupture.

Once the west half of the beam lost the continuity between the beam and slab, plastic hinging formed in the critical section at the west support of the middle loading truss (about 1 m from the beam centerline). This region was subjected to the maximum bending moment and the bearing stress from the point load. In this stage, both the beam and slab had their own neutral axes (each at their center of gravity). The beam failed by yielding and a flexural crack was developed through the depth of concrete slab (Figure 9c). The legs of west angles welded to the column sacrificial plate were completely detached at the peak load of the third cycle (Figure 9d), which was the same as the limit state of angle connections (i.e., weld shear) designed using AISC design table.

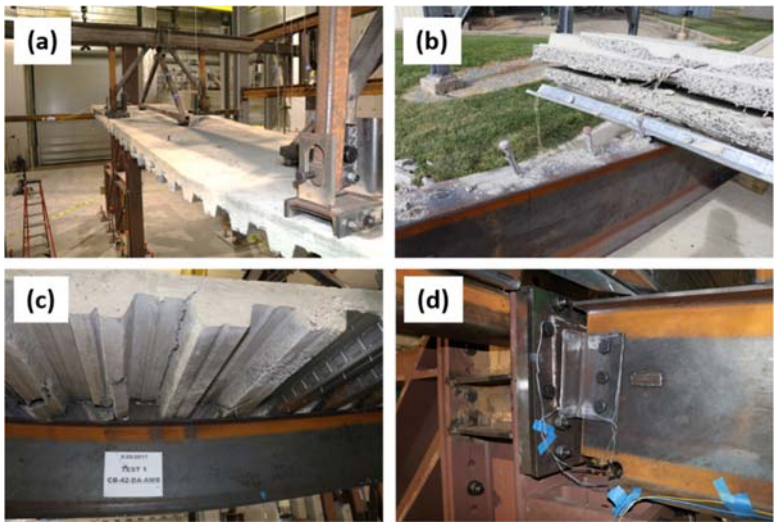

Figure 9 (a) failure of composite action at the west side of specimen, (b) exposed shear studs after the test, (c) exposed concrete at 1 m left of beam centerline, and (d) west connection after the test.

SUMMARY AND CONCLUSIONS

This paper presents the results of an ambient temperature composite beam test recently conducted at NIST. The specimen was nominally 13 m long and supported by steel columns via AISC bolted/welded double-angle connections. The data produced by this test will serve as the baseline for subsequent tests on composite beams with combined mechanical and fire load, as well as to validate computational models.

Failure initiated at the west end of the beam at the interface between the shear studs and the concrete when the specimen was subjected to a symmetric bending moment about its strong axis. Subsequently, flexural plastic hinging occurred near midspan of the beam (about 1 m to the west of the beam center). The test was terminated when fracture occurred in the welds on the double-angle connection at the west end of the beam. A peak load capacity of 63 ± 6.1 kN was achieved with a corresponding midspan deflection of approximately 100 mm. The gap between the beam web and the column flange varied during loading, but never fully closed. Processing of strain data measured in the slab and the beam is ongoing.

ACKNOWLEDGEMENTS

The support of numerous NIST colleagues on this work is acknowledged and greatly appreciated: Brian Story, Anthony Chakalis, Laurean DeLauter, Philipp Deardorff, Matthew Bundy, Artur Chernovsky, Doris Rinehart, Chao Zhang, Mina Seif, Qi Li, Ana Sauca, Dale Bentz, Scott Jones, Timothy Barrett, Max Peltz, Kevin McGrattan, Morgan Bruns, Randy Shields, Fahim Sadek, Joe Main, Jonathan Weigand, and Jian Jiang. The authors would like to thank Alana Guzetta of US Concrete who prepared the concrete mix design, as well as Roberto Talavera of Superior Concrete who supervised the casting. Expertise on fiber optic instrumentation was provided by Genda Chen, Yi Bao, Steve Guo, Matthew Klegseth, Branko Glisic, and John Reilly.

REFERENCES

Alfawakhri, F., Carter, C., Berhing, R., Zeeveld, P., Hervey, & F., Woods, L. (2016). "The Effects of Load Intensity and Restraint on the Fire Resitance of Steel and Composite Beams", proc of the 9th International Conf. Structures in Fire, Princeton, NJ.

ASTM International. (2017) "Standard Test Method for Compressive Strength of Cylindrical Concrete Specimens", *ASTM. C39/C39M − 17b*, ASTM International, West Conshohocken, PA, 2017

ASTM International. (2016) "Standard Test Methods for Tension Testing of Metallic Materials", *ASTM.E8/E8M-16a*, ASTM International, West Conshohocken, PA, 2016, doi:10.1520/E0008_E0008M-16A

Bundy, M., Hamins, A., Gross, J., Grosshandler, W., and Choe, L. (2016). "Structural fire experimental capabilities at the NIST National Fire Research Laboratory," Fire Technology, 52(4), 959-966.

Choe, L., Ramesh, S., Hoehler, M., Seif, M., Bundy, M., Zhang, C., and Gross, J. (2017). "National Fire Research Laboratory Commissioning Project: Testing Steel Beams under Localized Fire Exposure", NIST TN 1977, DOI: https://doi.org/10.6028/NIST.TN.1977

Flint, G., Lamont, S., Lane, B., Sarrazin, H., Lim, L., Rini, D., and Roben, C. (2013). "Recent lessons learned in structural fire engineering for composite steel structures", Fire Technology, 49(3), 767-792.

NIST (2008). Final Report on the Collapse of World Trade Center Building 7, Federal Building and Fire Safety Investigation of the World Trade Center Disaster (NIST NCSTAR 1A)

Selden, K. L., Fischer, E. C., & Varma, A. H. (2015). "Experimental investigation of composite beams with shear connections subjected to fire loading". Journal of Structural Engineering, 142(2), 04015118.

Taylor, B. N., and Kuyatt, C. E. (1994). "Guidelines for Evaluating and Expressing the Uncertainty of NIST Measurement Results." NIST Technical Note TN-1297, Gaithersburg, MD.

Wellman, E. I., Varma, A. H., Fike, R., and Kodur, V. (2011). “Experimental evaluation of thin composite floor assemblies under fire loading. Journal of Structural Engineering”, 137(9), 1002-1016.